



Strategies for 1D compression testing of large particle sized Tire Derived Aggregate (TDA)

Journal:	<i>Geotechnical Testing Journal</i>
Manuscript ID	GTJ-2017-0091.R3
Manuscript Type:	Technical Manuscript
Date Submitted by the Author:	n/a
Complete List of Authors:	Adesokan, Doyin; University of Saskatchewan, Civil, Geological and Environmental Engineering Fleming, Ian; University of Saskatchewan, Civil, Geological and Environmental Engineering Hammerlindl, Adam; University of Saskatchewan, Civil, Geological and Environmental Engineering McDougall, J.; Edinburgh Napier University
ASTM Committees and Subcommittees:	D20.10.24 Engineering and Design Properties < D20 Committee on Plastics
Keywords:	Geotechnics of Sustainable Construction, Tire derived aggregate (TDA), Waste disposal sites, Landfill drainage, Leachate collection and removal systems, Large strains, 1D compression, Sidewall friction, Large sized consolidometer, Laboratory testing
Abstract:	<p>Laboratory testing of a mass of large particle sized Tire Derived Aggregate (TDA) to assess performance related properties such as void ratio, compressive creep and hydraulic conductivity under large loads poses a number of experimental challenges. Large particle sized TDA is shredded scrap tires with particle sizes from 50 mm to over 305 mm. The large particle size of the TDA mass results in experimental challenges, such as the need for a large test chamber and the need for a load application system with a capacity to apply and sustain large loads, while accommodating large vertical displacements from the compression of the TDA sample mass.</p> <p>As an example, to put these requirements into perspective, a mass of TDA with a nominal particle size of 150 mm requires a test cell diameter of at least 600 mm and preferably 700 mm diameter. If a load of 400 kPa were to be applied onto the TDA mass to simulate approximately 35 m to 40 m of overlying material (waste and routinely applied cover materials) in an application such as a landfill, the test apparatus must be capable of delivering over 150 kN of applied load.</p> <p>Furthermore, for a reasonable initial mass of TDA that is 1.2 m thick, the test cell will have to be designed to maintain that load through over 0.6 m of vertical displacement due to the compression of the TDA mass. This paper presents a number of practical strategies that were implemented to overcome the experimental challenges with testing large particle size,</p>

1
2
3
4
5
6
7
8
9
10
11
12
13
14
15
16
17
18
19
20
21
22
23
24
25
26
27
28
29
30
31
32
33
34
35
36
37
38
39
40
41
42
43
44
45
46
47
48
49
50
51
52
53
54
55
56
57
58
59
60

	highly compressible TDA mass to establish the performance related properties for use in service. The focus of this paper is on equipment design and experimental methodologies and a few sample results from the study are presented to illustrate the successful implementation of the design methodologies.

SCHOLARONE™
Manuscripts

For Review Only

Strategies for 1D compression testing of large particle sized Tire Derived Aggregate (TDA)

Doyin Adesokan*¹, Ian Fleming¹, Adam Hammerlindl¹ and John McDougall²

ABSTRACT

Laboratory testing of a mass of large particle sized Tire Derived Aggregate (TDA) to assess performance related properties such as void ratio, compressive creep and hydraulic conductivity under large loads poses a number of experimental challenges. Large particle sized TDA is shredded scrap tires with particle sizes from 50 mm to over 305 mm. The large particle size of the TDA mass results in experimental challenges, such as the need for a large test chamber and the need for a load application system with a capacity to apply and sustain large loads, while accommodating large vertical displacements from the compression of the TDA sample mass.

As an example, to put these requirements into perspective, a mass of TDA with a nominal particle size of 150 mm requires a test cell diameter of at least 600 mm and preferably 700 mm diameter. If a load of 400 kPa were to be applied onto the TDA mass to simulate approximately 35 m to 40 m of overlying material (waste and routinely applied cover materials) in an application such as a landfill, the test apparatus must be capable of delivering over 150 kN of applied load.

Furthermore, for a reasonable initial mass of TDA that is 1.2 m thick, the test cell will have to be designed to maintain that load through over 0.6 m of vertical displacement due to the compression of the TDA mass. This paper presents a number of practical strategies that were

¹ Department of Civil, Geological & Environmental Engineering, University of Saskatchewan, 57 Campus Drive, Saskatoon SK Canada

² School of Engineering & the Built Environment, Edinburgh Napier University, 10 Colinton Road, Edinburgh

*Corresponding author: ada477@mail.usask.ca

1
2
3 implemented to overcome the experimental challenges with testing large particle size, highly
4 compressible TDA mass to establish the performance related properties for use in service. In
5
6 some instances, components of the test equipment had to be re-engineered to accommodate
7
8 exigencies that had not been anticipated, such as differential compression of the TDA mass. The
9
10 focus of this paper is on equipment design and experimental methodologies and a few sample
11
12 results from the study are presented to illustrate the successful implementation of the design
13
14 methodologies. Although TDA has been studied in this work, the strategies described herein can
15
16 be applied to a wide range of highly compressible materials under large loads.
17
18
19
20
21
22
23

24 **Keywords**

25
26 Scrap tire, tire derived aggregate, tire shreds, landfill, 1D consolidometer, creep, drainage
27
28 blanket, large strains, solid waste, and highly compressible materials
29
30
31
32

33 **Introduction**

34
35 Over the past two decades, in large part for economic considerations and as a means for
36
37 re-using the large stream of scrap tires generated at the end of the useful life of automobile tires,
38
39 TDA derived from shredding scrap tires into sizes from 25 mm to over 305 mm has been
40
41 suggested (Hall 1991; Duffy, 1995; Reddy and Saichek, 1998; Warith et al. 2004), researched
42
43 (McIsaac and Rowe, 2005; Rowe and McIsaac, 2005; Hudson et al. 2007; Beaven et al. 2007;
44
45 Beaven et al. 2013) and used (Donovan et al. 1996; Evans, 1997; Zimmerman, 1997; Reddy and
46
47 Saichek, 1998; Warith et al. 2004) as a substitute for gravel in the blanket drainage layers of
48
49 leachate collection and disposal systems. In the western Canadian provinces of Saskatchewan
50
51 and Alberta, TDA is used in over thirty landfills that receive between a quarter and a third of the
52
53
54
55
56
57
58
59
60

1
2
3 combined municipal solid waste stream of the two provinces.
4
5
6

7
8 TDA is a polymeric composite, as such a mass of TDA subjected to vertical loading is
9
10 expected to exhibit viscoelastic behavior (Reddy and Marella 2001; Warith et al, 2004) typically
11
12 consisting of an immediate elastic spring-like response followed by a time dependent viscous
13
14 dashpot-like response (creep). It is important to understand both responses and their individual
15
16 and combined effects on long-term performance and service life when designing load-bearing
17
18 applications such as drainage layers in waste disposal sites with TDA. The performance and
19
20 service life of any drainage layer is expected to exceed the contaminating lifespan of the waste
21
22 disposal facility, which has been estimated to be several centuries (Rowe and Fleming 1998;
23
24 Fleming et al. 1999; Fleming and Rowe. 2004; Rowe 2005; Yu and Rowe 2012). This expected
25
26 service life and performance depends on a number of factors including: (1) The ability of the
27
28 drainage layer to maintain a sufficient vertical and more importantly horizontal permeability to
29
30 rapidly transmit infiltrating leachate from the overlying waste into collection pipes and sumps to
31
32 minimize excessive head on basal barrier materials (Fleming et al. 1999; Qian et al. 2002; Rowe
33
34 et al. 2004; Yu and Rowe 2012); (2) The ability of the drainage layer to retain a sufficient pore
35
36 volume following physical and inevitable biogeochemical clogging to ensure continuous
37
38 transmission of leachate into collection and removal units (Fleming et al. 1999; Qian et al. 2002;
39
40 Rowe and McIsaac 2005; Rowe and Babcock 2007; Beaven et al. 2013); (3) The ability of the
41
42 drainage layer to transfer vertical load to underlying basal barrier materials without inducing or
43
44 making worse localized strains and other forms of physical damage (Dickinson and Brachman
45
46 2008).
47
48
49
50
51
52
53
54
55
56
57
58
59
60

1
2
3 Various studies such as Hall 1991; Reddy and Saichek 1998; Warith et al. 2004, Rowe
4 and McIsaac 2005; McIsaac and Rowe 2005 have shown that different TDA samples (differing
5 in terms of shape, particle size, mode of shredding, exposed and loose wire content) perform
6 differently in compression under similar applied loads and loading conditions. Strenk et al (2007)
7 highlighted the variability and scale dependence of TDA particle size and performance related
8 properties. Similarly, studies by Beaven et al (2007), Mwai et al (2010) and Beaven et al (2013)
9 showed that particle size matters in the behavior of a TDA mass under applied loads.
10
11
12
13
14
15
16
17
18
19
20

21 The 1D compression results presented in the Beaven and Mwai studies showed that TDA
22 masses with large sized particles (particles greater than 200 mm) compressed more than those
23 with smaller sized particles (200 mm and less) under similar applied loads. A higher
24 compression implies a higher void volume reduction and void volume reduction is a key
25 parameter for assessing the performance of TDA in service, especially for drainage applications
26 under service loads. For these reasons, testing smaller particle sized TDA in smaller test
27 equipment to eliminate the need for large sized testing equipment may result in errors in
28 estimating the performance and service life of large particle sized TDA.
29
30
31
32
33
34
35
36
37
38
39
40

41 In assessing the service life of a TDA mass for drainage applications in waste disposal
42 sites under high compressive loads imposed by overlying materials, it is imperative to perform
43 the required tests on a TDA mass with particle sizes and attributes that are suitable for such
44 applications. Ideally, large particle sized TDA with longest particle dimension from 50 mm to
45 over 305 mm. Testing such large sized particles will require large test cells and large systems for
46 applying and sustaining high compressive loads on the test cells.
47
48
49
50
51
52
53
54
55
56
57
58
59
60

1
2
3 Laboratory testing of a mass of TDA with large sized particles requires the use of large-
4 scale testing equipment and this may present a number of challenges. Zimmerman (2007)
5 appeared to have alluded to this in the study in which 200 mm to 400 mm particle sized TDA
6 mass were tested. The author stated that it was “impractical” to have a test chamber several times
7 larger than the largest particle size. “Practicality” as stated by Zimmerman could have been
8 related to potential challenges associated with having a large sized test chamber and in the study;
9 a smaller test chamber equal in width to the longest TDA particle dimension was used.
10
11
12
13
14
15
16
17
18
19
20

21 Testing a sample mass of TDA in a chamber with the same dimensions as the longest
22 particle size may increase sidewall friction along the walls of the test chamber. Sidewall friction
23 is an artefact of 1D constrained loading tests (Olson, 1986; Sarby and Vickers, 1986) and given
24 the flexibility of TDA particles there is an increased tendency for them to stick to the walls of
25 test cells potentially increasing sidewall friction. Sidewall friction reduces the amount of applied
26 load reaching the bottom of the test sample, causing larger strains in materials at the top of the
27 test cell than at the bottom (Sarby and Vickers, 1986).
28
29
30
31
32
33
34
35
36
37
38
39

40 Sidewall friction has been noted to increase as the ratio of chamber size to longest TDA
41 particle dimension decreases (ASTM D6270-08). The effects of sidewall friction could result in
42 erroneous estimation of the properties of the TDA mass potentially causing an underestimation
43 of compression and overestimation of porosity in the TDA mass if unaccounted for in the
44 analyses of the laboratory test results.
45
46
47
48
49
50
51
52
53

54 It was deemed important from the outset to be able to measure and account for sidewall
55
56
57
58
59
60

1
2
3 friction. Since sidewall friction was anticipated to be significant, the stress state could be
4
5 expected to vary across the thickness of the sample in the consolidometer. Accordingly, it was
6
7 deemed necessary to measure the total vertical stress reaching the base of the sample and to
8
9 estimate the compression at intermediate positions within the TDA mass.
10
11
12
13

14
15 Because the test cell was fabricated from transparent acrylic, colored lacrosse balls were
16
17 placed as visual markers at intermediate levels to enable the test sample to be treated as if it were
18
19 a stack of thinner slices each subjected to differing vertical and horizontal stress conditions. In
20
21 later tests, the colored balls were replaced by fluorescent paint spots applied to individual
22
23 particles of TDA placed near the cylinder sidewall. In order to determine the actual vertical
24
25 stress reaching the base of the TDA mass, a total stress (TS) cell was placed on the acrylic base
26
27 of the apparatus prior to filling with TDA.
28
29
30
31
32

33
34 Each slice created by a top and bottom visual marker thus may be considered to represent
35
36 a compression test at an applied load. The progression of compression in each slice was
37
38 measured from the displacement of the visual markers and each slice was analyzed as an
39
40 individual compression test at the applied load reaching the slice. The vertical stress reaching
41
42 each slice was estimated from considerations of sidewall friction along with the observed
43
44 variation in vertical strain and the measured total stress at the base of the sample.
45
46
47
48

49
50 Evaluating the performance determining properties of large particle sized TDA under
51
52 large applied and sustained vertical loads is the basis of a series of completed and ongoing
53
54 studies at the University of Saskatchewan (U of S), Canada. Two pieces of custom, large-scale
55
56
57
58
59
60

1
2
3 laboratory testing equipment – a 1D consolidometer and a 2D consolidometer/permeameter unit
4
5 were designed and fabricated at the U of S as part of these studies.
6
7
8
9

10 The equipment and procedures for the 1D consolidometer for evaluating compression,
11 creep and ensuing void ratio reduction in the TDA mass are described in this paper. The 2D
12 consolidometer/permeameter unit was used to evaluate the effects of void volume reduction on
13 horizontal and vertical permeability under increasing applied vertical load; this equipment and
14
15
16
17
18
19 the experimental methodologies employed will be discussed in a complementary paper.
20
21
22
23

24 The equipment design and experimental methodologies for the 1D consolidometer are
25 presented in this paper as a series of technical challenges that were overcome in order to
26
27
28
29
30
31
32
33
34
35
36
37
38
39
40
41
42
43
44
45
46
47
48
49
50
51
52
53
54
55
56
57
58
59
60

The challenges described include:

- The geometry of the test chamber and the associated structural considerations given the large particle size of the test sample
- A system for applying and sustaining high loads on the test sample under large compressive strains
- Managing differential compression in the heterogeneous TDA sample mass
- Measuring phase (solid and void) volume change under increasing applied loads
- Measuring and reducing sidewall friction

1
2
3 In view of the above, the three fold objectives of this paper are to: (1) describe the design
4 aspects of the 1D consolidometer and the experimental challenges that were encountered; (2)
5 describe the strategies that were developed and implemented to overcome these challenges; and
6 (3) present some test results from the implementation of the experimental designs and test
7 equipment.
8
9
10
11
12
13
14
15
16

17 Material

18
19
20
21
22 The TDA used in this study (Fig. 1) was supplied by Shercom industries, Saskatoon
23 Saskatchewan. Shercom produces TDA from scrap passenger and light truck tires.
24
25
26
27
28

29 Quantitative analyses were performed to determine the particle size distribution (PSD) and
30 specific gravity of the TDA mass. For the PSD, approximately 20 kg of TDA was selected
31 randomly and the length, width, thickness and mass of each individual shred was measured. Plots
32 of PSD using the cumulative percentage smaller than the longest dimension of each shred and
33 the cumulative percentage smaller than the smallest dimension of each shred are presented in
34 Figs. 2 a and b. The specific gravity of the test samples was measured according to ASTM C127
35 – 12 to be 1.27.
36
37
38
39
40
41
42
43
44
45
46

47 CHALLENGE 1: A SUITABLE TEST CHAMBER

48
49 Given the large dimensions of the TDA particles, a large test chamber several times larger in
50 diameter than the longest dimension of the test sample was required to minimise sidewall friction
51 as recommended in ASTM D6270-08. In addition, the height of the test chamber had to be
52
53
54
55
56
57
58
59
60

1
2
3 sufficient to accommodate an initially greater thickness of a mass of TDA that would undergo
4
5 large compressive strains as loading progressed.
6
7

8
9
10 **A** 1.8 m high 1D consolidometer with a diameter of 0.7 m was fabricated from a cylinder of
11
12 transparent acrylic material with wall thickness of 0.1 m and ultimate tensile strength of
13
14 approximately 50 MPa and an elastic modulus of 3.2 GPa (Fig. 3a). In the load frame, the
15
16 consolidometer was placed on a wooden base plate of the same diameter as the outer diameter of
17
18 the consolidometer; the base plate had sufficient clearance underneath for a forklift to move the
19
20 consolidometer in and out of the load frame. A schematic of the 1D consolidometer setup with
21
22 details of the load application system is presented in Fig. 3b.
23
24
25
26
27

28
29 It was important to be able to move the consolidometer in and out of the loading frame with
30
31 minimal obstructions and to have a load frame that was sufficiently sturdy with adequate
32
33 capacity to withstand applied loads. It was also important to have a system for loading and
34
35 unloading the consolidometer. A triangular design was implemented for the load frame to
36
37 facilitate easy movement of the consolidometer in and out of the load frame (Fig. 3a), and a
38
39 gantry system allowing for various degrees of inclination of the consolidometer was fabricated
40
41 for loading and unloading the consolidometer (Fig. 4)
42
43
44
45
46

47 **CHALLENGE 2: THE LOADING SYSTEM**

48
49 The large sized consolidometer meant a large loaded area, **the application of large vertical loads**
50
51 **of over 150 kN** and a loading system capable of applying and maintaining the large vertical loads
52
53 constantly at high strains greater than 50%. A loading system such as this would require a long
54
55
56
57
58
59
60

1
2
3 extension stroke with means for lowering and raising the system, whilst maintaining constant
4
5 load on the test sample.
6
7
8
9

10 In addition, components that would facilitate the transfer and distribution of the applied vertical
11 load uniformly across the surface of the test sample in the consolidometer were required. To
12
13 apply the large constant loads, 21 ½-inch diameter stock units of double convolution air bellows
14
15 (model 9109150) were sourced from Parker-Hannifin. The air bellows were subsequently
16
17 modified by removing the factory fitted upper and lower plates - items “f” and “h” in Fig. 5a and
18
19 replacing them with steel plates and gusset reinforcement (Fig. 5b) to enhance the load bearing
20
21 capacity of the air bellows and prevent excessive bending of the inset ring plates during loading.
22
23
24
25
26
27

28 The re-engineered air bellows (Fig. 5b) weighs 123 kg and has the capacity to generate over 150
29
30 kN, which could be used to apply vertical stresses up to 600 kPa. The maximum applied vertical
31
32 stress in the testing described in this paper was 224 kPa to simulate 20 m to 25 m of overlying
33
34 waste (Zekkos et al. 2006) above a mass of TDA in a landfill drainage application.
35
36
37
38
39

40 A 0.04 m by 1.64 m piston rod fabricated out of steel was used to transfer the load from the air
41
42 bellows to the loading plate on the test sample. The loading plate was fabricated from the same
43
44 acrylic material as the consolidometer, is 20 mm thick and is 5 mm smaller in diameter than the
45
46 inner diameter of the consolidometer, providing sufficient clearance along the walls of the
47
48 consolidometer during loading.
49
50
51
52
53

54 A piston guide was incorporated into the loading system to provide alignment for the piston rod
55
56
57
58
59
60

1
2
3 during loading. Both the piston guide and air bellows were connected to the load frame by upper
4 and lower “arms” that were attached to threaded rods bolted onto the top of the load frame (see:
5
6 Figure 3b). The length of threaded rods was designed to allow for sustained loading on the TDA
7
8 mass over a total displacement associated with vertical strains exceeding 50%.
9

10
11
12
13
14 The “arms” were manually wound down while maintaining constant pressure in the air bellows
15
16 by means of pressure relief valves. This ensured that a constant load was supplied to the TDA
17
18 mass as the applied vertical stress increased and compressive strains became larger.
19
20
21
22
23

24 **A button-type load cell with a capacity of over 150 kN sourced from Futek Inc. (model LLB500)**
25
26 was positioned between the lower end of the piston rod and the press plate to determine the
27
28 actual load supplied by the air bellows to the consolidometer. The load cell was placed in a
29
30 housing and this was bolted to the top of the press plate to ensure that the load cell was held in
31
32 place during the tests. The load cell was connected to a PC controlled readout unit and the
33
34 vertical load supplied to the test sample was displayed in real time.
35
36
37
38
39

40 A pancake type VW total stress (TS) cell (P/N 52608220, S/N 11-1282) with a capacity **of over**
41
42 **300 kPa** manufactured by Durham Geo Slope Indicator (DGSI) was used to measure the load
43
44 reaching the bottom of the consolidometer. **The TS cell readings were useful for estimating the**
45
46 **effectiveness of the sidewall treatments that were applied to the walls of the 1D consolidometer**
47
48 **for reducing sidewall friction. They were also useful for developing a theoretical approach for**
49
50 **estimating the loss of applied surface load across the thickness of the TDA mass resulting from**
51
52 **sidewall friction.**
53
54
55
56
57
58
59
60

1
2
3
4
5 The TS cell was placed in the 1D consolidometer prior to filling with TDA, resting flat on the
6 rigid base of the consolidometer to avoid poor conformance and stiffness-compatibility related
7 errors in the total stress measurement that may occur with placing the TS cell within the TDA
8 mass. A description of poor conformance and stiffness compatibility errors in total stress
9 measurements is provided in Dunicliff (1988).
10
11
12
13
14
15
16
17
18

19 A 25 mm thick plywood disc the same diameter as the TS cell was placed on top of the TS cell
20 before loading the consolidometer with TDA to ensure an even distribution of applied stresses on
21 the TS cell. The TS cell was connected to a VW Data recorder (P/N 52613500, S/N 42182) by
22 DGSI to obtain readings.
23
24
25
26
27
28
29
30

31 **CHALLENGE 3: DIFFERENTIAL COMPRESSION**

32
33 Because of the variations in shapes and sizes of the particles in the TDA mass, and an initially
34 large void volume from the large sizes of the TDA particles, differential compression and
35 misalignment of the load application system occurred at the early stages of the testing. Following
36 an increase of load from 112 kPa to 224 kPa, uneven settlement of the TDA mass occurred, and
37 this caused the press plate to tilt and the piston rod misaligned such that only a small portion of
38 the lower end of the piston rod was left in contact with the load cell.
39
40
41
42
43
44
45
46
47
48

49 A diagnostic evaluation of the occurrence showed that the clearance between the piston rod and
50 the annulus of the piston guide was insufficient and this had caused the piston rod to bind at the
51 ends of the piston guide during the misalignment (Fig. 6a). This binding resulted in significant
52
53
54
55
56
57
58
59
60

1
2
3 fluctuations in the load reaching the surface of the TDA mass.
4
5
6

7
8 The piston guide that was originally used had been a linear bearing cartridge placed inside a
9
10 cylindrical canister base. Embedded inside the cartridge were rings of small sized ball bearings
11
12 to provide alignment of the piston rod. The linear bearing design provided motion and full
13
14 contact in the direction of the cartridge, but did not allow for misalignment of the piston rod. The
15
16 piston guide had to be redesigned and re-fabricated to accommodate deflections and
17
18 misalignments in subsequent tests.
19
20
21
22
23

24 The redesigned piston guide has an annular single row consisting of 5/8 sized ball bearings to
25
26 provide a single point of contact around any given point of the piston rod. The ball bearings in
27
28 the piston guide are capped in two halves that are bolted together to form a canister base. The
29
30 redesigned piston guide provides better alignment and freer movement of the piston rod, and is
31
32 able to accommodate misalignments up to 15°, creating a diametric clearance of almost 3 mm
33
34 within the annulus of the piston guide.
35
36
37
38
39

40 In addition to redesigning the piston guide, the lower end of the piston rod was fitted with a
41
42 cylindrical hollow base having a conical tip to create a wider contact area between the lower end
43
44 of the piston rod and the surface of the load cell during misalignment. With the conical tip
45
46 attachment, the piston rod is able to revolve or rotate on the load cell during differential
47
48 settlements and misalignments without slipping off completely (Fig. 6b).
49
50
51
52
53

54 With the re-engineered piston assembly, during subsequent testing, the piston rod was able to
55
56
57
58
59
60

1
2
3 move freely within the annulus of the piston guide and was able to misalign slightly without
4 binding at the edges of the piston guide, while maintaining maximum contact with the load cell.
5
6
7 The re-engineered piston assembly reduced the fluctuations in applied load reaching the test
8 sample during subsequent tests considerably.
9
10
11
12
13

14 **CHALLENGE 4: MEASURING COMPRESSIVE STRAINS AND VOID VOLUME** 15 **REDUCTION** 16 17

18
19 There are currently no standard test methods for evaluating compression and void volume
20 reduction in a mass of TDA under applied loads. Standard methods for evaluating creep in
21 polymers ASTM D2990 – 09, and ASTM D7406 – 07 were adapted as required.
22
23
24
25
26
27

28 **Evaluating Solid Volume Compression in TDA Particles** 29

30
31 Before setting out to measure the compression and void volume reduction in the TDA mass, it
32 was deemed essential to identify the contribution of solid volume compression in individual
33 TDA particles to the overall void volume reduction, so that appropriate means for evaluating the
34 resulting void volume reduction may be established. A complementary study was completed as
35 part of this research work to evaluate the contribution of solid volume compression of individual
36 TDA particles to overall compression and creep.
37
38
39
40
41
42
43
44
45
46

47 In that study, isotropic stresses from 50 kPa, to 200 kPa were applied incrementally to a mass of
48 TDA in a 0.6 m by 0.3 m triaxial cell for over 90 days. Upon application of load, there appeared
49 to be some elastic compression, but subsequently there was little or no further compression over
50 the test period to the end of the final isotropic stress of 200 kPa.
51
52
53
54
55
56
57
58
59
60

1
2
3
4
5 Given the minimal solid volume compression observed in that study, it was determined that void
6
7
8 volume reduction may be the principal mechanism for compressive strains in a mass of TDA
9
10 under applied loads and compressive solid volume change in the individual TDA particles may
11
12 be ignored. Hence, any change in void volume in a mass of TDA under applied loads may be
13
14 represented by the change in sample height using Eq 1.
15

$$\frac{\Delta H}{H} = \frac{\Delta e}{1+e_0} \text{ and } \Delta V_s = 0 \quad (1)$$

16
17
18
19
20 Where:

21
22 H = height

23
24 e = void ratio and

25
26
27 V_s = volume of solids.
28
29
30

31 **Measuring 1D Compression and Change in Void Volume in the TDA mass – Primary** 32 33 **Strategy**

34
35
36 Having fabricated the consolidometer cell from transparent plastic, it was possible to place visual
37
38 markers at various depths within the test sample and the vertical displacement of the markers
39
40 could be tracked periodically to measure intermediate strains. A set of three colored four-inch
41
42 diameter balls with a comparable elastic modulus to the modulus of individual TDA particles
43
44 were placed at predetermined heights as visual markers against the inside walls of the
45
46 consolidometer adjacent to three 1.8 m long measuring tapes that had been glued to the outside
47
48 wall of the cell 120 degrees apart.
49
50

51
52
53
54 The position of the visual markers was read across the measuring tapes as loading progressed.
55
56
57
58
59
60

1
2
3 Adjacent visual markers separated the test sample into intermediate slices. The slices were
4 analyzed to represent series of tests running simultaneously in the test cell. The mass of TDA
5 placed in each slice separated by the visual markers was determined during loading and since the
6 specific gravity of the TDA had been previously measured, the dry unit weight of each mass of
7 TDA slice was estimated. Knowing these, it was possible to estimate the initial void volume in
8 the slices and the change in void volume with the progression of the test using Eq 2.
9
10
11
12
13
14
15

$$e = \left(\frac{G_s \gamma_w}{\gamma_{dry}} \right) - 1 \quad (2)$$

16
17
18
19
20 Where:

21
22 G_s = specific gravity

23
24 γ_w = the unit weight of water (kN/m^3)

25
26
27 γ_{dry} = the unit weight of dry TDA mass in the slices (kN/m^3)
28

29 **Measuring 1D Compression and Change in Void Volume in the TDA mass – Auxillary** 30 **Strategy** 31 32

33
34 Drainable porosity was measured periodically as an auxiliary method for estimating compression
35 and change in void ratio within the TDA mass. Drainable porosity measurements for void ratio
36 evaluation in a mass of TDA has been done by previous researchers e.g. McIsaac and Rowe
37 (2005), Rowe and McIsaac (2005), Hudson et al (2007).
38
39
40
41
42
43
44
45

46 The fabrication of the consolidometer included threaded ports at the base for introducing fluids
47 into the test sample. The threaded ports made it easy to remove the fittings when not in use to
48 recover a smooth flush base for transporting the cell around on a forklift. The ports were barb
49 fitted to allow for connection of flexible tubing for fluid flow. The barb fitting design was to
50 ensure a smooth flush on the inside of the consolidometer at the base and to prevent intrusion of
51
52
53
54
55
56
57
58
59
60

1
2
3 fittings into the consolidometer or standing water at base during drainable porosity tests.
4
5
6

7
8 Both filling and draining porosities were evaluated in the drainable porosity tests. For the filling
9
10 porosity, a graduated cylinder was placed on a scaffold and a flexible tubing was connected to
11
12 the bottom of the graduated cylinder and to the ports at the bottom of the 1D consolidometer.
13
14 The tubing connection allowed water to drain by gravity from the graduated cylinder into the 1D
15
16 consolidometer for filling porosity measurements. Water from the graduated cylinder flowed
17
18 under gravity to fill up the consolidometer to the elevation of the visual markers and the
19
20 transparent cell made it easy to see the water level rise to the required elevation. .
21
22
23

24
25
26 The consolidometer was filled from bottom to top to ensure saturation of the TDA mass for the
27
28 measurements. Each TDA mass slice was filled within 24 hours – this period may not have been
29
30 sufficient to ensure complete saturation of the voids in the TDA mass. Because of this, the void
31
32 ratio measurements from drainable porosity presented in this paper may have underestimated the
33
34 values slightly. A comparison of the void ratio values from drainable porosity and those from
35
36 measuring the displacement of the visual markers is presented later on.
37
38
39

40
41
42 For the draining porosity, the consolidometer cell was drained by gravity into the graduated
43
44 cylinder and it was observed that draining the cell too quickly resulted in delayed drainage.
45
46 Delayed drainage is a situation whereby water from preceding layers, if not allowed enough time
47
48 to drain completely, seeps into lower layers while draining those layers.
49
50

51
52
53 Delayed drainage ultimately results in erroneous readings of draining porosity because lower
54
55
56
57
58
59
60

1
2
3 layers would drain a larger volume of water, while upper layers would drain a lesser volume of
4 water and the void volume in the various layers would be misrepresented. To manage delayed
5 drainage during the draining porosity tests, a constant head container was attached to the load
6 frame and a flexible tubing was connected to the top of the constant head container and the ports
7 at the bottom of the 1D consolidometer (Fig. 7).
8
9
10
11
12
13
14
15
16

17 The constant head container was lowered to predetermined heights - usually the height of the
18 visual markers and water from the 1D consolidometer drained by gravity into the constant head
19 container through the flexible tubing. Overflow from the constant head container was collected
20 into the graduated cylinder and when the head of water in the 1D consolidometer was equal to that
21 of the water inside the constant head container, the set up was left undisturbed for a few hours to
22 collect any delayed drainage from upper layers.
23
24
25
26
27
28
29
30
31
32

33 Following the drainable porosity tests, filling and draining porosity values of the TDA mass
34 slices were determined using Eq 3. Corresponding void ratio values were estimated from the
35 porosity values.
36
37
38
39

$$40 \quad n = V_{water} / V_{TDA} \quad (3)$$

41
42
43 Where:

44 n = porosity

45 V_{water} = volume of water

46 V_{TDA} = volume of the TDA mass slice filled or drained
47
48
49
50
51
52
53
54

55 **CHALLENGE 5: MANAGING SIDEWALL FRICTION**

56
57
58
59
60

Sidewall Friction Reduction

In the conventional 1D oedometer standard testing procedure ASTM D2435 / D2435M - 11, test cell, to minimize sidewall friction, height - to - sample diameter ratios of 1:2.5 are recommended and height-to-diameter ratios greater than 1:4 are preferred. The height to diameter ratio of the 1D consolidometer used in this study was 2.5:1, significant sidewall friction was anticipated because of this and methods for reducing and accounting for sidewall friction were required.

Two treatment methods for reducing sidewall friction were evaluated. Treatment 1 involved applying a layer of high temperature grease to the inside walls of the consolidometer and placing a layer of 0.15 mm polyethylene plastic on top of the greased wall. Treatment 2 involved applying two layers of the same plastic and two layers of the high temperature grease to the inside walls of the consolidometer. The grease was applied directly to the wall of the consolidometer and in between the two layers of plastic.

Both treatments resulted in over 50% reduction in sidewall friction as shown in the sample results for an applied load of 112 kPa (Table 1) for readings from the TS cell placed beneath the TDA mass in the consolidometer. Treatment 2 achieved a slightly higher reduction and was applied in subsequent tests.

TABLE 1: EFFECTS OF SIDEWALL FRICTION TREATMENTS AT 112 kPa

Operation	% load reaching the bottom at 112 kPa
No sidewall treatment	46%

Treatment 1	50%
Treatment 2	54%

Sidewall Friction Evaluation

Despite applying sidewall treatments, it may not be possible to eliminate sidewall friction in 1D constrained testing of a TDA mass. With this in mind, an approach that may be used to evaluate sidewall friction loss to enable a detailed evaluation of the compression behavior of the test sample for design was developed and is presented here. The evaluation approach presented in this study is similar to a theoretical approach that was previously developed by Beaven (2000) from the testing of municipal solid waste.

The Beaven approach relates the vertical effective stress (σ'_v) at a depth z in the cell to the internal angle of friction (ϕ') of the waste and to the interface shear friction angle (δ) between the waste and the wall of the test cell. The Beaven approach assumed that ϕ' , δ and the unit weight (γ) of the waste were constant with applied load and depth and the resulting equation was given as:

$$\sigma'_v = \frac{\gamma}{B} (1 - e^{-Bz}) + P \cdot e^{-Bz} \quad (4)$$

Where

$$B = \left[\frac{4(1 - \sin \phi') \cdot \tan \delta}{d} \right]$$

P = the applied surface load

Although the theoretical approach by Beaven and the approach presented in this paper share some similarities, the techniques that were applied to develop the resulting equations are

1
2
3 different. In the Beaven approach, there was a reliance on the internal angle of friction of the
4 waste sample and the actual stress reaching the bottom of the test cell and intermediate strains
5 within slices of the test sample were not measured.
6
7
8
9

10
11
12 In addition, in the Beaven approach the unit weight of the TDA mass was assumed to be
13 constant. This assumption of a constant unit weight may result in errors in estimating the void
14 ratio with applied loads and with depth. This is because the unit weight of a mass of TDA will
15 depend on the applied loads and the resulting compression from the applied loads.
16
17
18
19
20
21
22

23
24 Additionally, since the applied loads in a constrained loading test of a TDA mass will vary
25 across the thickness of the sample mass because of sidewall friction, the unit weight of the TDA
26 mass will not be constant throughout the sample. Thus, assuming a constant unit weight with
27 applied load and sample thickness for the TDA mass may result in errors in estimating the effects
28 of sidewall friction, and additionally cause a misrepresentation of the void volume reduction in
29 the TDA mass with applied stress.
30
31
32
33
34
35
36
37
38
39

40 The sidewall friction equation presented in this paper considers intermediate slices of the TDA
41 mass and evaluates the compression and void volume change in each slice. As such, the equation
42 accounts for the changes in unit weight with depth across the thickness of the TDA mass and
43 presents a range of sidewall friction angle (δ) values for various applied loads that were obtained
44 from the test results. The sidewall evaluation equation and approach in this study are described in
45 the following sections.
46
47
48
49
50
51
52
53
54
55
56
57
58
59
60

The parameters governing sidewall friction were determined using the load cell readings at the top, intermediate strains measured from the displacement of the visual markers and the TS cell readings beneath the TDA mass. Using these readings it was possible to integrate applied load with depth and to evaluate strains at any point within the TDA mass to account for sidewall friction loss.

In the evaluation procedure, sidewall friction was assumed to be analogous to the Mohr-Coulomb model that may be used to evaluate interface shear resistance given in Eq 5.

$$\tau = K_o \sigma'_z \tan \delta + c_a \quad (5)$$

Where

τ = shear stress

K_o = lateral "earth" pressure coefficient

σ'_z = applied vertical stress

$\tan \delta$ = angle of interface shearing resistance

c_a = adhesion

It was assumed that K_{oTDA} and $\tan \delta$ were constant with depth giving a first order decay of vertical stress with depth as follows:

$$\sigma'_{z(z)} = \sigma_{z_0} e^{(-4K_{oTDA} \tan \delta z / D)} \quad (6)$$

Where:

$\sigma'_{z(z)}$ = vertical load at a particular depth,

$\sigma_{z(0)}$ = the applied vertical load at the top

K_{oTDA} = lateral pressure coefficient for a TDA mass

1
2
3 δ = the interface shearing angle between the TDA mass and the walls of the test cell
4

5 Z = the depth from the applied stress
6

7 D = the diameter of the test cell
8
9

10
11
12 Since the applied load at the top ($\sigma_{z(0)}$) and the stress reaching the bottom of the sample were
13 known, the term $K_{oTDA} \tan \delta$ that is analogous to the parameter β for skin friction of piles was
14 estimated from a simple root mean square error (RMSE) analysis. The parameters K_{oTDA} and
15 $\tan \delta$ were subsequently separated and determined independently from specific individual
16 measurements. These measurements are described in the following sections.
17
18
19
20
21
22
23
24
25

26 The RMSE analysis of top and bottom stresses in the TDA mass yielded a $K_{oTDA} \tan \delta$ value of
27 0.75 for no sidewall friction treatment and 0.12 for sidewall friction treatment 2. To estimate the
28 value of K_{oTDA} , the hoop strain was measured in the thick-walled acrylic test cylinder and this
29 value was used with a 3D finite element (FE) model of the acrylic test cell as described in the
30 following paragraphs. The focus of the FE modelling and independent direct shear tests
31 completed was to determine approximate values of K_{oTDA} and $\tan \delta$ that may tease out the
32 lumped β parameter and not for a detailed analysis of the TDA mass.
33
34
35
36
37
38
39
40
41
42
43
44

45 *Estimation of K_{oTDA}*

46

47 Three high precision strain gauges were glued to the outer wall of the consolidometer 120° apart
48 at a height corresponding to the region of estimated maximum hoop strain upon increasing
49 applied load. The strain gauges were connected to a read out unit and resultant hoop strains were
50 recorded as vertical stresses increased.
51
52
53
54
55
56
57
58
59
60

1
2
3
4
5 A 3D FE model was developed for the consolidometer apparatus using the software package
6
7 Abaqus. The mechanical response of the acrylic cylinder was simulated using a linear elastic
8
9 model for small strains in acrylic in order to estimate the value of K_{oTDA} by adjusting the
10
11 horizontal earth pressure of the TDA to match the hoop strain values measured by the strain
12
13 gauges on the sidewalls of the apparatus. The TDA itself was not explicitly part of the FE model
14
15 except in that the outward horizontal stress applied by the vertically loaded mass of TDA was
16
17 applied as a load boundary condition to the surface of the acrylic cylinder. This outward
18
19 horizontal stress decreased with height along this boundary in accordance with the vertical stress
20
21 distribution $\sigma'_z(z)$ throughout the TDA mass and the shear stress distribution $\tau_z(z)$ along the
22
23 walls of the consolidometer (Fig. 8).
24
25
26
27
28
29
30

31 The FE model was run multiple times using Eqs 5 and 6 and the thickness of the TDA mass. The
32
33 value of K_{oTDA} was varied until the hoop strain predicted by the FE model matched the observed
34
35 values. The resulting best-fit value of K_{oTDA} obtained using the FE model was 0.7. It should be
36
37 noted that a mass of TDA is not a perfectly homogeneous isotropic linearly elastic material and
38
39 representing the lateral and shear stress from the TDA mass as a boundary condition for the FE
40
41 model of the acrylic cylinder is necessarily a simplification. The FE modelling did yield a
42
43 reasonable value of K_{oTDA} for the analyses. Furthermore, the value was useful for estimating the
44
45 maximum load that may be safely applied to a TDA mass in the test apparatus without the risk of
46
47 damaging the acrylic cylinder.
48
49
50
51
52
53

54 *Estimation of $\tan \delta$*
55
56
57
58
59
60

1
2
3 Using $K_{OTDA} = 0.7$, a RMSE analysis was applied to vary the value of $\tan \delta$ in Eq 6 until the
4
5 calculated measurements at the bottom of the cell matched the readings from the TS cell at the
6
7 bottom of the TDA mass. The estimated value of δ from this approach was between 10° to 12°
8
9 for the applied loads.
10
11
12

13
14 For an independent evaluation of $\tan \delta$, testing was conducted in a 300 mm by 450 mm direct
15
16 shear box to determine an approximate value for the interface friction angle δ between the TDA
17
18 mass and the walls of the acrylic test cell with sidewall treatment 2 applied. The applied normal
19
20 stresses and sidewall conditions in the 1D consolidometer were simulated as closely as possible.
21
22

23
24 It should be noted that the dimensions of the TDA particles (ranging from 50 mm to 305 mm)
25
26 being close to the direct shear box dimensions could have resulted in edge effects between the
27
28 TDA particles and the walls of the direct shear box. This may have contributed to the interface
29
30 shear friction values recorded for the TDA mass and acrylic interface.
31
32

33
34
35 Another aspect of the direct shear test to point out is that the plastic layers were replaced and
36
37 grease layers were re-applied for each test in the direct shear box. These were not done in the
38
39 compression tests in the 1D consolidometer; the initial grease layers and plastic applied in the 1D
40
41 consolidometer were used from start to finish of the compression tests. As such, the δ values that
42
43 were determined independently in the direct shear box may have underestimated the friction
44
45 values. The results from the direct shear interface friction tests are presented in Table 2.
46
47
48
49
50

51
52 **TABLE 2 - RESULTS FROM THE MEASUREMENT OF δ° WITH SIDEWALL**
53
54 **TREATMENT 2**
55
56
57
58
59
60

Applied stress, $\sigma(z)$, kPa	shear stress τ , kPa	$\tan \delta$	δ°
39.4	3.8	0.01	0.7
65.3	5.9	0.04	2.3
195.0	9.4	0.03	1.8
255.0	10.9	0.03	1.7
304.4	12.1	0.03	1.7

The results from the evaluation approaches for δ as described in the preceding sections suggest that $\tan \delta$ may not depend on the applied stress significantly. This may substantiate the premise that δ may be assumed to be constant with depth in the formulation of the sidewall evaluation strategy for evaluating stress distribution within the test sample presented in Eq 6. The values of δ estimated from measurements in the 1D consolidometer were higher than the values from the individual direct shear tests in Table 2.

The higher δ values may be related to the ripping of the plastic sidewall liners with increased loading causing direct contact (sticking) of some TDA particles to the wall of the consolidometer. This may have caused non-uniform displacements along the TDA mass and wall interface, potentially increasing the sidewall friction compared with the direct shear tests in which the plastic layers were replaced for each test run and had fewer rips.

Notwithstanding, since the vertical stress applied to each “slice” was known, and the compressive response of the TDA had been determined across a range of loads, it was important

1
2
3 to have a good estimate of the degree to which sidewall friction changed the vertical stress from
4
5 the top to the bottom of the sample. However, had the sidewall friction effect been more or less
6
7 pronounced, the results in the 1D consolidometer would have still been usable as long as a good
8
9 estimate of the distribution of vertical stress could be made.
10
11
12
13
14

15 Discussion

16 17 IMMEDIATE COMPRESSION AND CREEP

18
19 The progression of compression at the applied surface loads of 112 kPa and 224 kPa, simulating
20
21 approximately 10 m to 25 m of waste above the drainage layer respectively are presented in
22
23 Fig.9. Compression in the TDA mass as measured periodically from the vertical displacement of
24
25 Fig.9. Compression in the TDA mass as measured periodically from the vertical displacement of
26
27 the colored visual markers are presented in Fig. 10 - where H1 to H5 are the labels for the visual
28
29 markers from the topmost marker H1 to the bottom marker H5.
30
31
32
33

34 The initial positions of the visual markers (H1 to H5) before applying the 112 kPa surface load
35
36 were H1 = 1.78 m, H2 = 1.42 m, H3 = 1.06 m, H4 = 0.72 m, H5 = 0.32 m. At both load steps of
37
38 112 kPa and 224 kPa, there was a large immediate compression followed by some creep (Table
39
40 3).
41
42

43 TABLE 3 - IMMEDIATE AND TIME DEPENDENT COMPRESSION OF THE TDA 44 45 MASS 46 47 48 49 50 51 52 53 54 55 56 57 58 59 60

Applied top stress (kPa)	Overall compression (%)	Immediate compression (%)	Time dependent compression (%)
112	44	41.5	2.5
224	Additional 10.5	7.8	2.7

The total compression at the end of the final load step of 224 kPa was approximately 55% and the contribution of creep to this was approximately 5%. Immediate sample compression upon application of the loads was larger at 112 kPa and reduced significantly at the 224 kPa load step. This is indicative of strain stiffening in the TDA mass with increased applied vertical stress. Strain stiffening in a TDA mass has been presented in studies by other researchers. For instance, the compression results presented by Beaven et al (2007) and Mwai et al (2010) for different sizes and types of TDA showed reduced compression – strain stiffening at stresses from 200 kPa and greater.

VOID RATIO EVALUATION

Before and after creep plots of void ratio with applied stress (e -log p plots) for the slices in the TDA mass, presented collectively as series of tests running concurrently are shown in Figure 11 (a). The onset of creep (in this study) is 24 hours after the application of the surface vertical load. Because of sidewall friction, the applied load at the top of the sample was reduced throughout the sample thickness and this resulted in a higher compression and void volume reduction in slices closer to the applied load than in slices farther away from it.

In addition to the Figure 11 (a) plots, e -log p plots for the end of creep for individual slices of the TDA mass, taking each slice as a separately run test and tracking the void ratio change in the

1
2
3 individual slices in relation to the applied surface loads are presented in Figure 11 (b). The void
4 ratio e was estimated using Eq 1, and the applied stress reaching the slice from the surface load
5
6
7
8 (p) was determined using Eq 6.
9

10
11
12 The void ratio in the top sample slice (H1 to H2) decreased by approximately 57% upon
13 application of the initial load of 112 kPa and further decreased by approximately 19% when the
14 applied load was increased from 112 kPa (end of creep) to 224 kPa. The void ratio reduction
15 induced by creep was approximately 10% at 112 kPa and 8% at 224 kPa. These were smaller
16 than the void ratio reduction induced by immediate compression before the onset of creep.
17
18
19
20
21
22
23
24
25

26 The shapes of the e - $\log p$ curves in Figs 11 a and b suggest that there may not be a unique
27 relationship between void ratio and applied loads for a mass of TDA as measured from
28 constrained loading. The void ratio of a TDA mass at a particular load appears to depend on the
29 loading stress path taken to get to that void ratio. Thus indicating that the compressive behavior
30 of a mass of TDA under controlled conditions may be complicated and there is need for field
31 measurements to calibrate laboratory test results.
32
33
34
35
36
37
38
39

40 **DRAINABLE POROSITY**

41
42 A representation of average drainable porosity and porosity estimated from the displacement of
43 the visual markers is presented in Fig. 12. The plot indicates some consistency between the void
44 ratio values estimated from drainable porosity and those estimated from the displacement of the
45 visual markers. However, the void ratio values that were estimated from drainable porosity
46 measurements appear to be generally lower than those estimated from the displacement of the
47 visual markers. This may be indicative of incomplete saturation of the TDA mass during the
48
49
50
51
52
53
54
55
56
57
58
59
60

1
2
3 filling process for drainable porosity.
4
5
6

7 The void ratio results in Fig. 12 further highlight the benefits of the primary approach, involving
8 the use of a transparent test cell and visual markers that was employed for measuring 1D
9 compression and void ratio in the TDA mass. Nonetheless, in the absence of a clear test cell,
10 drainable porosity values may still be used with a good degree of reliability to estimate void ratio
11 change in a TDA mass in compression tests. Filling of the TDA mass should be completed over a
12 longer period to potentially increase saturation and improve the accuracy of the measured values
13
14
15
16
17
18
19
20
21
22
23

24 **IMPLICATIONS OF CURRENT FINDINGS FOR PRACTICE AND FURTHER** 25 **COMPLETED AND ONGOING RESEARCH WORK ON TDA** 26

27 As stated in the preceding texts of this paper, the performance of a mass of TDA as the drainage
28 layer in waste disposal facilities depends on the porosity, permeability and pore volume of the
29 TDA mass following (1) compressive strains from overlying waste and cover materials, and (2)
30 biogeochemical clogging from leachate flowing through the drainage layer. The porosity of the
31 TDA mass under simulated overlying waste was evaluated in this study; this was found to reduce
32 by over 50% from an unloaded state to about 0.26 at the maximum applied load of 224 kPa.
33
34
35
36
37
38
39
40
41
42
43

44 Although the porosity of 0.26 at an applied load of 224 kPa – equivalent to between 20 m to 25
45 m of waste (Zekkos, 2006) may seem low, the coefficient of vertical and horizontal permeability
46 values of the TDA mass at a comparable porosity and applied stress have been evaluated and the
47 results show high permeability values for the TDA mass. The measured coefficient of vertical
48 and horizontal permeability of the TDA mass at an applied vertical stress of 219 kPa were 7.9E-
49
50
51
52
53
54
55
56
57
58
59
60

1
2
3 03 m/s and 1.9E-02 m/s respectively. These values are higher than the regulatory requirement of
4
5 1E-04 m/s in the Western Canada jurisdiction for a landfill drainage layer.
6
7
8
9

10 The details of the 2D permeability testing including equipment design and experimental
11 strategies employed will be presented in a companion paper. In addition, a porosimeter is being
12 used with image analysis to analyze the pore geometry of a sample mass of TDA under applied
13 vertical loading to obtain parameters such as specific surface, pore volume and pore size
14 distribution that may be used to evaluate the performance of a TDA mass against biogeochemical
15 clogging under various mass loading and flow scenarios. The findings from this study will be
16 presented in an upcoming paper.
17
18
19
20
21
22
23
24
25
26
27

28 Conclusions and Summary

29
30 The challenges with testing large particle size TDA for use under large stresses imposed by
31 overlying material have been discussed and some strategies for overcoming the challenges have
32 been presented. The highlights of this paper include the following:
33
34
35
36
37
38
39

- 40 1. Laboratory testing of large particle sized TDA is challenging and it unavoidably requires
41 the use of large sized test equipment with the capacity to apply large vertical loads and
42 accommodate large vertical strains.
43
44
- 45 2. The use of air bellows that can be wound down manually made it possible to apply and
46 sustain large loads onto the test sample while experiencing high vertical strains greater
47 than 0.5 m.
48
49
- 50 3. A mass of TDA with large sized particles has an initially large void volume that reduces
51
52
53

- 1
2
3 considerably upon loading because of a large immediate compression and some creep.
4
5
6 4. Compression in a mass of TDA has been determined to be from void volume reduction
7
8 and the compression of individual solid particles may be ignored.
9
10
11 5. The use of a clear “see through” consolidometer provided the opportunity to measure
12
13 intermediate strains and void ratio in slices within the test sample. A single test can
14
15 therefore yield information regarding a range of stresses concurrently if intermediate
16
17 strains in slices are measured.
18
19
20 6. There is a need for unconstrained field-testing of TDA mass samples to eliminate the
21
22 effects of sidewall friction and to calibrate laboratory test data obtained from constrained
23
24 1D compression testing.
25
26
27 7. It is essential to account for sidewall friction in the laboratory testing of TDA to avoid
28
29 overestimating the applied stresses and void ratio throughout the test sample. For
30
31 instance, if methods for measuring and estimating sidewall friction such as using a clear
32
33 test cell, placing visual markers at intermediate levels to separate the test sample into
34
35 slices, placing a TS cell at the bottom of the sample to account for sidewall friction loss,
36
37 and using a theoretical model to estimate applied stresses in intermediate sample slices
38
39 were not employed, the actual applied stresses within the sample thickness, the resulting
40
41 strains and void volume reduction may have been overestimated. Dividing the test
42
43 sample into slices and determining the applied stress and void ratio in each slice made is
44
45 possible to determine the actual void ratio at an applied stress following the effects of
46
47 sidewall friction.
48
49
50
51 8. The sidewall friction evaluation approach that was presented in this paper can be used to
52
53 estimate stresses and strains at any point within the consolidometer, potentially
54
55
56
57
58
59
60

eliminating the need for TS cells beneath the test sample.

9. Void volume reduction in a TDA mass was found to reduce significantly as applied vertical stresses increased. This confirms the strain stiffening behavior of a mass of TDA under applied loads, , substantiating similar findings from previous researchers (e.g. Beaven et al., 2007; Mwai et al., 2013)

10. Nonlinearities in the e - $\log p$ consolidation curves indicate that the 1D constrained creep compression of a mass of TDA might be complicated.

11. Although TDA has been tested in this study, the strategies that were implemented in this study may be applicable to a wide range of highly compressible materials with an initially large void volume that would reduce significantly following compressive displacements under vertical loading.

ACKNOWLEDGMENTS

The equipment described in this paper was fabricated and subsequently modified by the University of Saskatchewan Engineering Machine Shops. The assistance and financial support of SNC-Lavalin and Shercom Industries is acknowledged.

REFERENCES

ASTM C127-12: Standard Test Method for Relative Density (Specific Gravity) and Absorption of Coarse Aggregate, ASTM International, West Conshohocken, PA, 2012,
www.astm.org

1
2
3 ASTM D2435 / D2435M - 11: Standard Test Methods for One-Dimensional Consolidation

4
5 Properties of Soils Using Incremental Loading, ASTM International, West

6
7 Conshohocken, PA, 2011, www.astm.org

8
9
10 ASTM D2990-09: Standard Test Methods for Tensile, Compressive, and Flexural Creep and

11
12 Creep Rupture of Plastics, ASTM International, West Conshohocken, PA, 2009,

13
14
15 www.astm.org

16
17
18 ASTM D6270-08: Standard Practice for Use of Scrap Tires in Civil Engineering Applications,

19
20
21 ASTM International, West Conshohocken, PA, 2008, www.astm.org

22
23
24 ASTM D7406-07: Standard Test Method for Time-Dependent (Creep) Deformation Under

25
26
27 Constant Pressure for Geosynthetic Drainage Products, ASTM International, West

28
29
30 Conshohocken, PA, 2007, www.astm.org

31
32 Beaven, R. P., 2000, "The hydrogeological and geotechnical properties of household waste in

33
34
35 relation to sustainable landfilling", *PhD Dissertation*, University of London, London,

36
37
38 England, pp. 81-89

39
40 Beaven, R. P., Hudson, A. P., Knox, K., Powrie, W., and Robinson, J. P., "Clogging of land fill

41
42
43 tyre and aggregate drainage layers by methanogenic leachate and implications for

44
45
46 practice," *Waste Management*, Vol. 33, 2013, pp. 431- 444

47
48 Beaven, R. P., Powrie, A. P., Hudson, A. P., and Parkes, D. J., "Compressibility of tyres for use

49
50
51 in landfill drainage systems," *Waste and Resource Management*, Vol. 159, No. WR4,

52
53
54
55
56
57
58
59
60 2007, pp. 173-180

- 1
2
3 Dickinson, S., and Brachman, R. W., "Assessment of alternative protection layers for a
4
5 geomembrane - geosynthetic clay liner (GM-GCL) composite liner", *Canadian*
6
7 *Geotechnical Journal*, Vol. 45, 2008, pp. 1594-1610
8
9
- 10 Donovan, R., Dempsey, J., and Owen, S., "Scrap tire utilization in landfill
11
12 applications," presented at the *17th Biennial Waste Processing Conference*, 1996, pp.
13
14 353-383
15
16
- 17 Duffy, D. P., "Using tire chips as leachate drainage layer," *Waste Age*, Vol. 26, No. 9, 1995, pp.
18
19 113-122
20
21
- 22 Dunicliff, J., *Geotechnical Instrumentation for Monitoring Field Performance*, John Wiley and
23
24 Sons, New York, 1988, pp. 165 -177
25
26
- 27 Evans, P., "Use of tire shred in landfill construction," presented at the *Geotechnical Society of*
28
29 *Edmonton Third Annual Symposium Environmentally Friendly Technologies in*
30
31 *Geotechnical Engineering*, Edmonton, Alberta, 1997, pp. 1-8
32
33
34
35
- 36 Fleming, I. R., and Rowe, R. K., "Laboratory studies of clogging of landfill leachate collection
37
38 and drainage systems," *Canadian Geotechnical Journal*, Vol. 41, 2004, pp. 134-158
39
40
- 41 Fleming, I. R., Rowe, R. K., and Cullimore, D. R., "Field observations of clogging in landfill
42
43 leachate collection systems," *Canadian Geotechnical Journal*, Vol. 36, 1999, pp. 605-
44
45 787
46
47
48
- 49 Hall, T. J., "Reuse of shredded tire material for leachate collection systems," presented at the
50
51 *14th Annual Madison Waste Conference*, University of Madison, Wisconsin, 1991, pp.
52
53 367-376
54
55
56
57
58
59
60

1
2
3 Hudson, A. P., Beaven, R. P., Powrie, W., and Parkes, D., "Hydraulic conductivity of tyres in
4 landfill drainage systems," *Waste and Resource Management*, Vol. 160, No. WR2, 2007,
5 pp. 63-70
6
7
8
9

10
11 McIsaac, R., and Rowe, K., "Change in leachate chemistry and porosity as leachate permeates
12 through tire shreds and gravel," *Canadian Geotechnical Journal*, Vol. 42, 2005, pp.
13 1173-1188
14
15
16
17

18
19 Mwai, M., Wichuk, K., and McCartney, D., "Implications of using Tire-derived Aggregate for
20 landfill leachate collection and drainage systems". In the *Proceedings of the Solid Waste*
21 *Association of North America, 5th Canadian Symposium* . Banff, Alberta, 2010, pp. 18-
22 21
23
24
25
26
27

28
29 Olson, R.E., "State of the Art: Consolidation Testing," *Consolidation of soils: testing and*
30 *Evaluation, ASTM STP 892*, R.N. Yong and F.C. Townsend, Eds., American Society for
31 Testing and Materials, Philadelphia, 1986, pp. 7-70.
32
33
34
35

36
37 Qian, X., Koerner, R. M., and Gray, D. H., 2002, *Geotechnical Aspects of Landfill Design and*
38 *Construction*, Prentice-Hall Inc., Upper Saddle River, New Jersey, pp. 294-330
39
40

41
42 Reddy, K. R., and Marella, A., "Properties of different size scrap tire shreds: Implications on
43 using as drainage material in landfill cover systems," presented at the *Seventeenth*
44 *International Conference on Solid Waste Technology and Management*, Philadelphia,
45 PA, USA, 2001, pp. 1-16
46
47
48
49

50
51 Reddy, K. R., and Saichek, R. E., "Characterization and performance assessment of shredded
52 scrap tires as leachate drainage material in landfills," presented at the *Fourteenth*
53
54
55
56
57
58
59
60

1
2
3 *International Conference on Solid Waste Technology and Management*, Philadelphia,
4
5 PA, USA, 1998
6
7

8 Rowe, K. R., and Babcock, D., "Modelling the clogging of coarse gravel and tire shreds in
9
10 column tests," *Canadian Geotechnical Journal*, Vol. 44, 2007, pp. 1273-1285
11
12

13 Rowe, K. R., and McIsaac, R., "Clogging of tire shreds and gravel permeated with landfill
14
15 leachate," *Journal of Geotechnical and Geoenvironmental Engineering*, Vol. 131, 2005,
16
17 pp. 682-693
18
19

20
21 Rowe, R. K., "Long-term performance of contaminant barrier systems," *Geotechnique*, Vol. 55,
22
23 No. 9, 2005, pp. 631-678
24
25

26 Rowe, R. K., and Fleming, I. R., "Estimating the time for clogging of leachate collection
27
28 systems," presented at the *3rd International Congress: Environmental Geotechniques*,
29
30 Lisbon, Vol. 1, 1998, pp. 23-28.
31
32

33
34 Rowe, R. K., Quigley, R. M., Brachman, R. W., and Booker, J. R., 2004, *Barrier Systems for*
35
36 *Waste Disposal Facilities*, Taylor and Francis Books Ltd (E and FN Spon), London, pp.
37
38 587
39
40

41 Sarsby, R. W., and Vickers, B., "Side Friction in Consolidation Tests on Fibrous Peat,"
42
43 *Consolidation of Soils: Testing and Evaluation, ASTM STP 892*, R.N. Yong and F.C.
44
45 Townsend, Eds., American Society for Testing and Materials, Philadelphia, 1986,
46
47 pp.485-489.
48
49
50
51
52
53
54
55
56
57
58
59
60

1
2
3 Strenk, P. M., Wartman, J., Grubb, D. G., Humprey, D. N., and Natale, M. F., "Variability and
4
5 Scale-Dependency of Tire Derived Aggregate". *Journal of Materials in Civil*
6
7 *Engineering*, Vol. 19, 2007, pp. 233-241.

8
9
10 Warith, M. A., Evgin, E., and Benson, P., "Suitability of shredded tires for use in landfill
11
12 leachate collection systems," *Waste Management*, Vol. 24, 2004, pp. 967-979

13
14
15
16 Wartman, J., Natale, M. F., and Strenk, P. M., "Immediate and time dependent compression of
17
18 tire derived aggregate," *Journal of Geotechnical and Geoenvironmental Engineering*,
19
20 Vol. 133, No. 3, 2007, pp. 245-256

21
22
23 Yu, Y., and Rowe, K. R., "Modelling leachate-induced clogging of porous media," *Canadian*
24
25 *Geotechnical Journal*, Vol. 49, 2012, pp. 877-890

26
27
28
29 Zekkos, D., Bray, J. D., Kavazanjian, E. J., Matasovic, N., Rathje, E. M., Reimer, M. F., and
30
31 Stokoe II, K. H., "Unit Weight of Municipal Solid Waste," *Journal of Geotechnical and*
32
33 *Geoenvironmental Engineering*, Vol. 132, 2006, pp. 1250-1261

34
35
36 Zimmerman, P. S., 1997, "Compressibility, Hydraulic Conductivity and Soil Infiltration of Tire
37
38 Shreds and Field Testing of a Shredded Tire Horizontal Drain," *MS Thesis*, Iowa State
39
40 University, Ames, Iowa

41 42 43 44 45 46 **List of Figure Captions**

47
48 **FIG. 1** TDA used in the study

49
50
51 **FIG. 2** Particle size distribution plots for the TDA mass using both longest and shortest
52
53 dimensions of individual particles

54
55
56 **FIG. 3 (a)** The 1D consolidometer placed in the triangular shaped load frame showing a
57
58
59

1
2
3 compression test in progress
4

5 **FIG. 3 (b)** Schematic of the 1D consolidometer and its components
6

7
8 **FIG.4** Gantry system for unloading and loading the consolidometer outside the load frame
9

10 **FIG. 5** (a) Components of re-engineered air bellows (b) Re-engineered air bellows with
11 gusset reinforcement
12
13

14 **FIG. 6 (a)** Representation of the initial piston guide design and deflection of the load
15 application system
16
17

18 **FIG. 6 (b)** Representation of the re-designed piston guide and deflection of the load
19 application system
20
21

22 **FIG. 7** Draining porosity test in progress showing the constant head addition (container)
23 for collecting delayed drainage during draining porosity.
24
25

26 **FIG. 8** A schematic representation of the consolidometer cell as it was used in the 3D FE
27 model to determine the value of K_{OTDA} for the TDA sample
28
29

30 **FIG. 9** Progression of the 1D compression test (a) no applied surface load (b) after
31 applying 112 kPa surface load (c) after applying 224 kPa surface load
32
33

34 **FIG. 10** Elevation of the visual markers at the applied surface loads of 112 kPa and 224
35 kPa. H1 to H5 are the labels for the visual markers from the topmost marker H1 to the bottom
36 marker H5. The initial positions of the visual markers (H1 to H5) before applying the 112 kPa
37 surface load are as follows: H1 = 1.78 m, H2 = 1.42 m, H3 = 1.06 m, H4 = 0.72 m, H5 = 0.32 m.
38
39

40 **FIG. 11 (a)** e - $\log p$ curves for the entire thickness of the TDA mass, treating the slices
41 collectively as a series of tests running concurrently. Adjacent visual markers in the test cell
42 formed individual slices – for instance, visual markers H1 to H2 formed the topmost slice and
43 visual marker H5 to the bottom of the cell formed the bottom slice. The applied loads in the
44
45
46
47
48
49
50
51
52
53
54
55
56
57
58
59
60

1
2
3 slices were estimated using Eq 6. The trend lines connecting circular markers on the plots
4 represent the before creep values and those connecting triangular markers represent after creep
5 values. The onset of creep in this study was taken as 24 hours after the applied load. The initial e
6 values in the slices before the 112 kPa surface load were H1 to H2 = 1.92, H2 to H3 = 1.92, H3
7 to H4 = 1.84, H4 to H5 = 1.71, H5 to the bottom of the cell = 1.51.
8
9

10
11
12
13
14 **FIG. 11 (b)** e - $\log p$ curves for individual slices of the TDA mass at the end of creep, treating
15 each slice as a separately run test and tracking the void ratio change in the individual slices for
16 the applied loads. For each slice there are three marker points indicated on the plot, the first
17 series of marker points indicate the initial void ratio values for each slice (under no external
18 applied loads, just the weight of overlying TDA mass), the second and third points indicate the
19 void ratio values at the end of 122 kPa and 224 kPa respectively.
20
21
22
23
24
25
26
27

28 **FIG. 12** Void ratio estimated from drainable porosity vs. void ratio from tracking the
29 vertical displacement (elevation) of the visual markers
30
31
32
33
34
35
36
37
38
39
40
41
42
43
44
45
46
47
48
49
50
51
52
53
54
55
56
57
58
59
60



FIG. 1 TDA used in the study

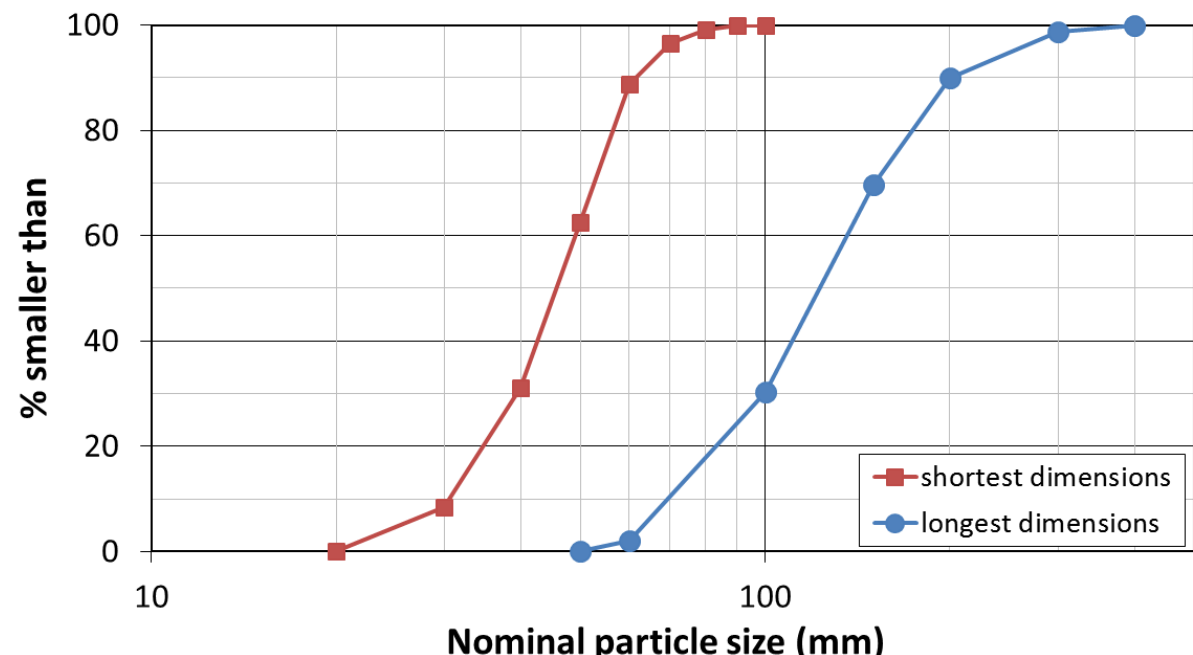


FIG. 2 Particle size distribution plots for the TDA mass using both longest and shortest dimensions of individual particles

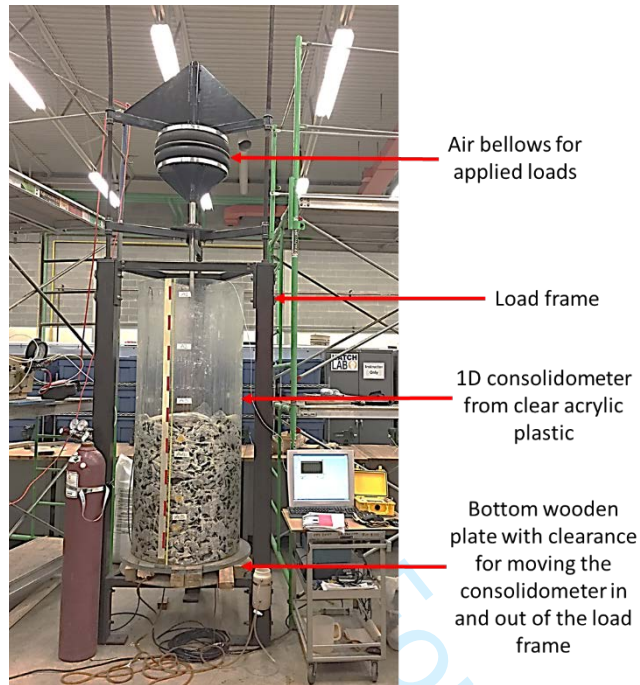


FIG. 3 (a) The 1D consolidometer placed in the triangular shaped load frame showing a compression test in progress

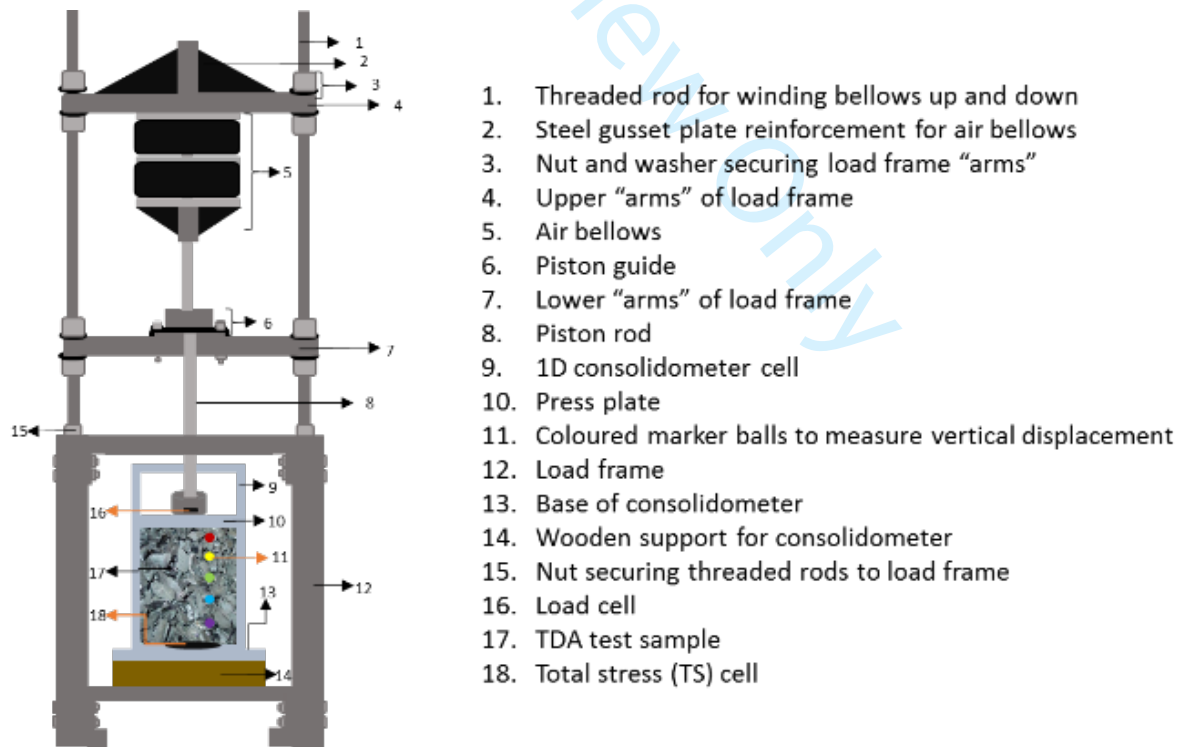


FIG. 3 (b) Schematic of the 1D consolidometer and its components

1
2
3
4
5
6
7
8
9
10
11
12
13
14
15
16
17
18
19
20
21
22
23
24
25
26
27
28
29
30
31
32
33
34
35
36
37
38
39
40
41
42
43
44
45
46
47
48
49
50
51
52
53
54
55
56
57
58
59
60



FIG.4 Gantry system for unloading and loading the consolidometer outside the load frame

For Review Only

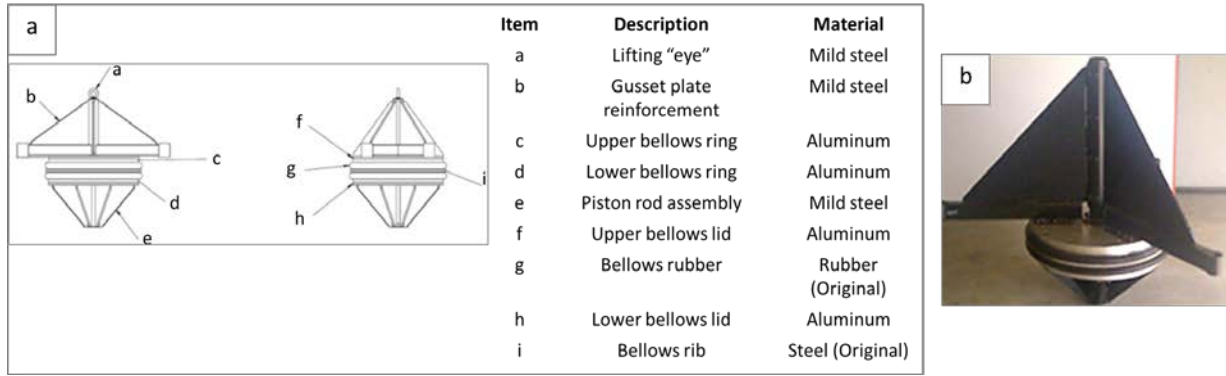


FIG. 5 (a) Components of re-engineered air bellows (b) Re-engineered air bellows with gusset reinforcement

For Review Only

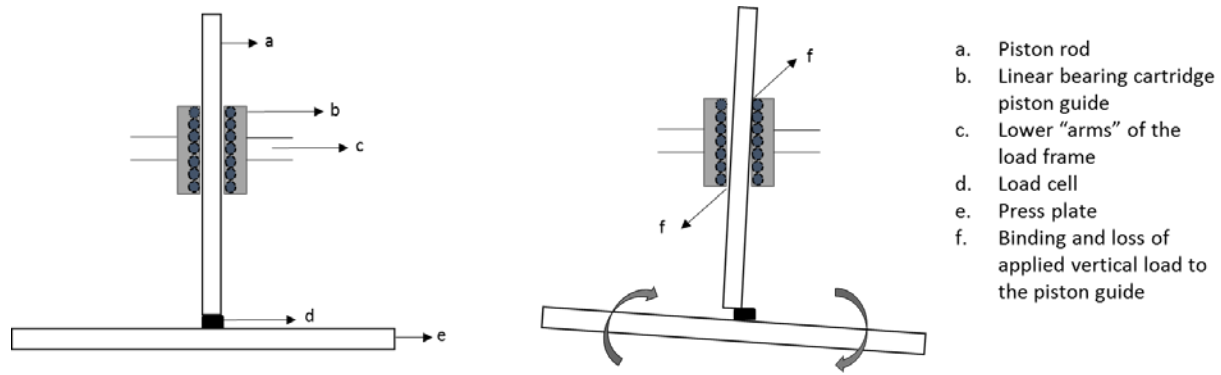


FIG. 6 (a) Representation of the initial piston guide design and deflection of the load application system

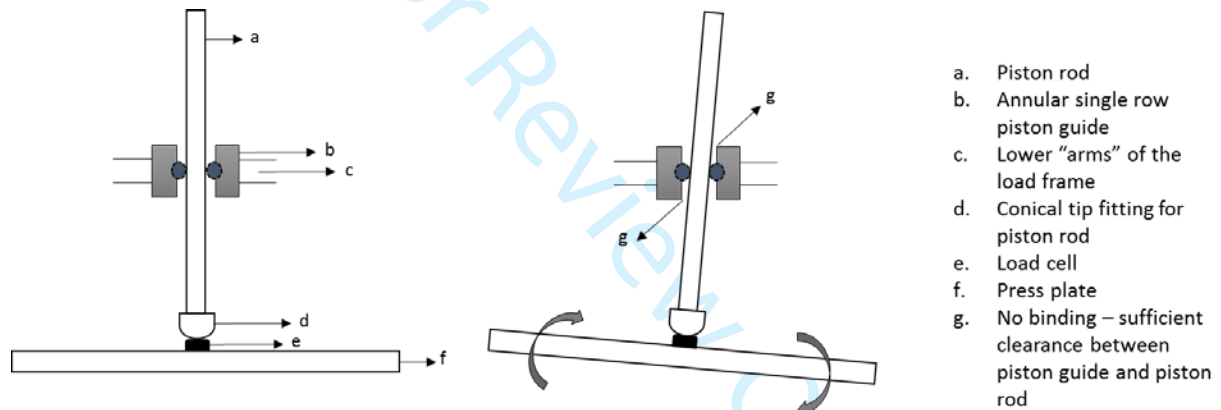


FIG. 6 (b) Representation of the re-designed piston guide and deflection of the load application system



FIG. 7 Draining porosity test in progress showing the constant head addition (container) for collecting delayed drainage during draining porosity

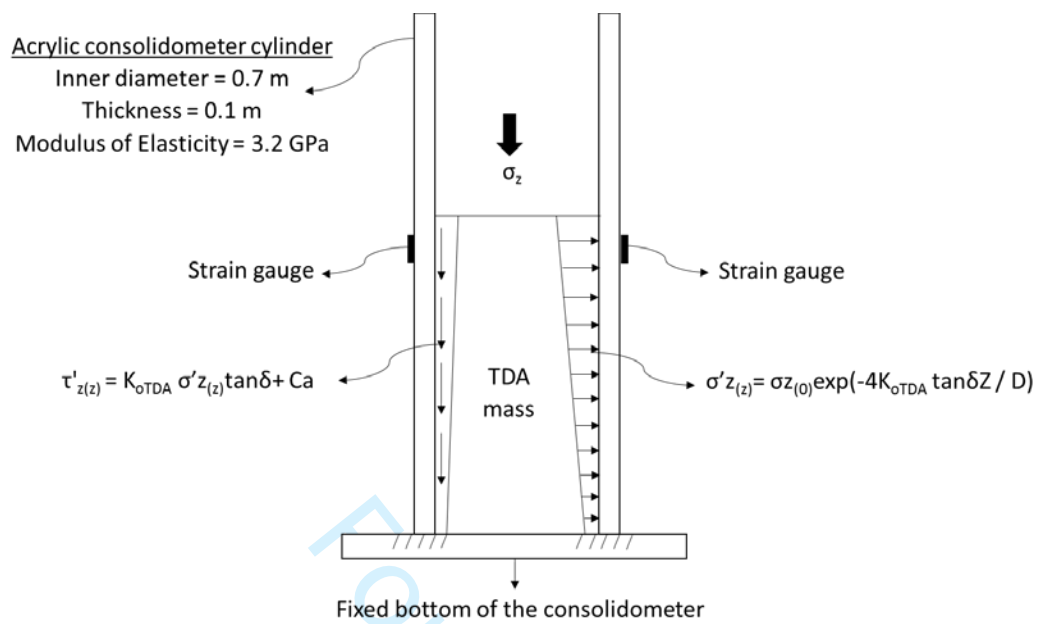


FIG. 8 Schematic of the consolidometer cell as it was used in the 3D FE model to determine the value of K_{oTDA} for the TDA mass

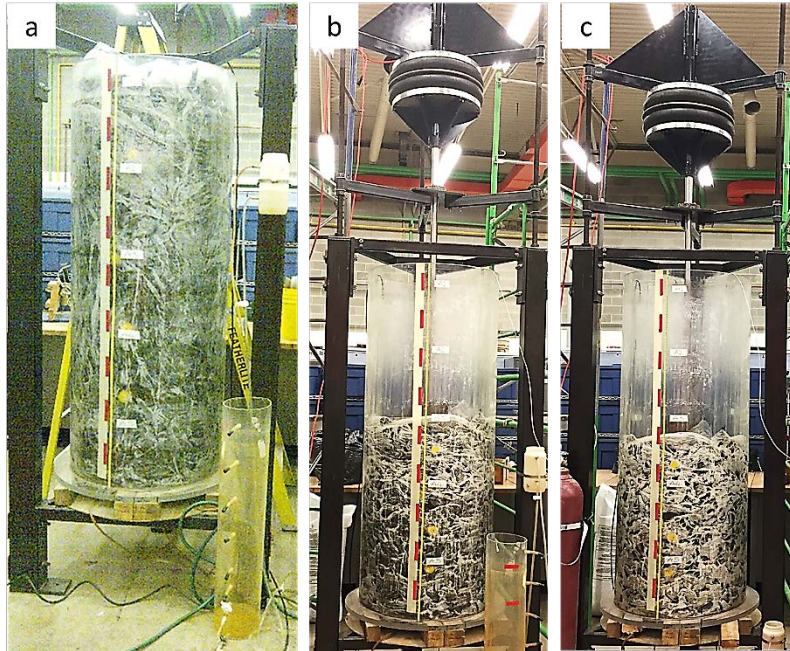


FIG. 9 Progression of the 1D compression test (a) no applied surface load (b) after applying 112 kPa surface load (c) after applying 224 kPa surface load

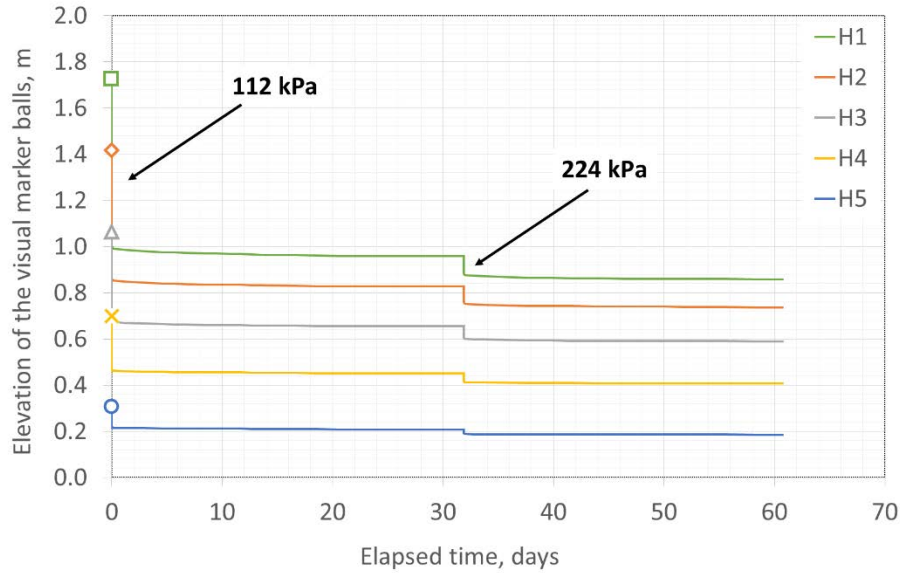


FIG. 10 Elevation of the visual markers at the applied surface loads of 112 kPa and 224 kPa.

H1 to H5 are the labels for the visual markers from the topmost marker H1 to the bottom marker H5. The initial positions of the visual markers (H1 to H5) before applying the 112 kPa surface load are as follows: H1 = 1.78 m, H2 = 1.42 m, H3 = 1.06 m, H4 = 0.72 m, H5 = 0.32 m.

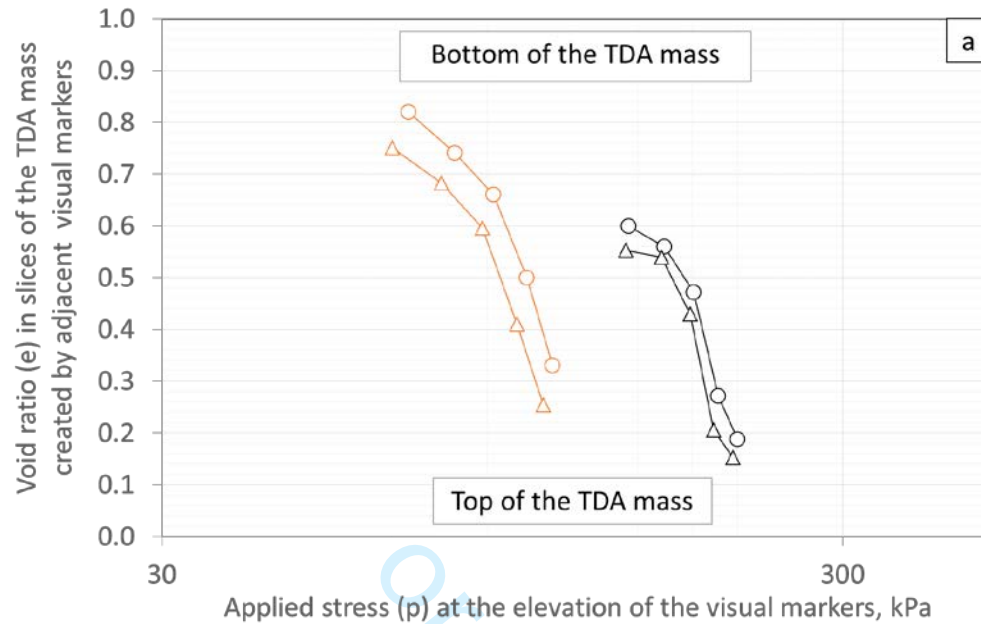


FIG. 11 (a) *e-logp* curves for the TDA mass taking the TDA mass slices collectively as a series of tests running concurrently. Adjacent visual markers in the test cell formed individual slices – for instance, visual markers H1 to H2 formed the topmost slice and visual marker H5 to the bottom of the cell formed the bottom slice. The applied loads in the slices were estimated using Eq 6. The trend lines connecting circular markers on the plots represent the before creep values and those connecting triangular markers represent after creep values. The onset of creep in this study was taken as 24 hours after the applied load. The initial *e* values in the slices before the 112 kPa surface load were H1 to H2 = 1.92, H2 to H3 = 1.92, H3 to H4 = 1.84, H4 to H5 = 1.71, H5 to the bottom of the cell = 1.51.

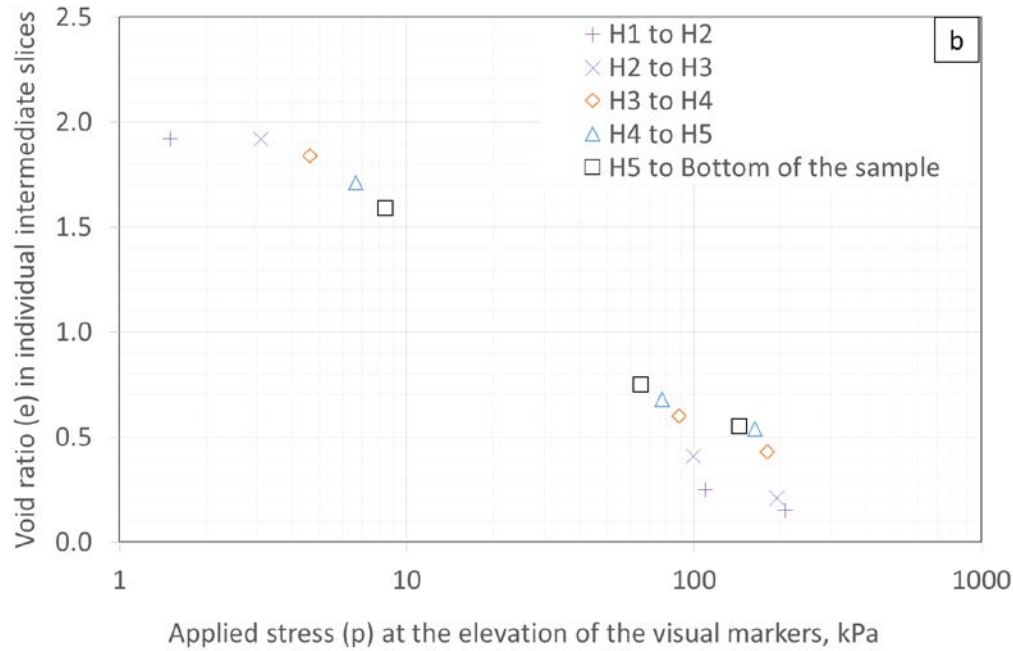


FIG. 11 (b) *e-logp* curves for individual slices of the TDA mass at the end of creep, treating each slice as a separately run test and tracking the void ratio change in the individual slices for the applied loads. For each slice there are three marker points indicated on the plot. The first series of marker points indicate the initial void ratio values for each slice (under no external applied loads, just the weight of overlying TDA mass). The second and third series of marker points indicate the void ratio values at the end of 122 kPa and 224 kPa respectively.

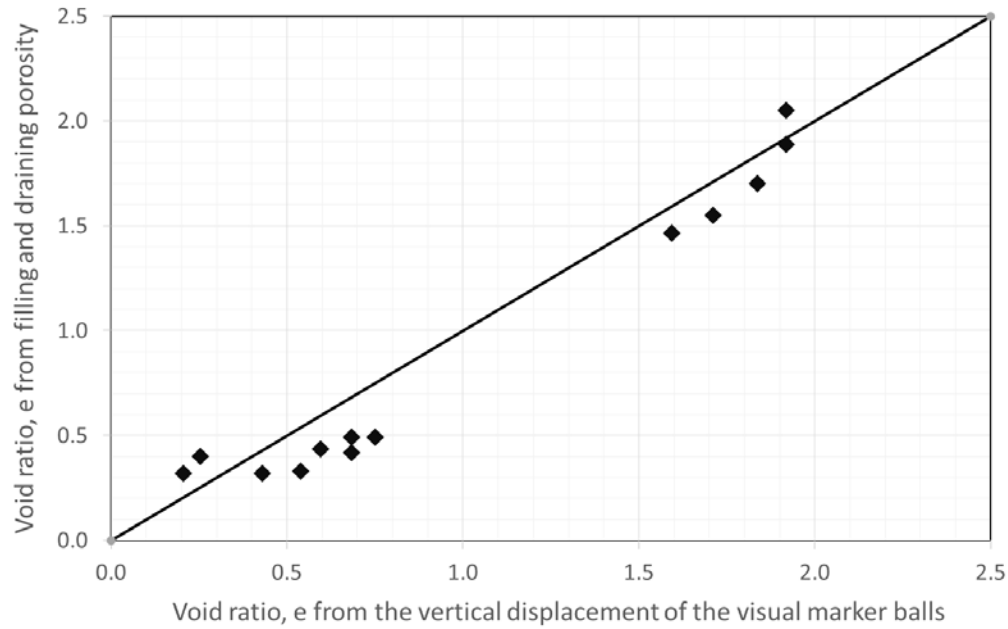


FIG. 12 Void ratio estimated from drainable porosity vs. void ratio from tracking the vertical displacement (elevation) of the visual markers